

3

**A Study of a Numerical Analysis on Three-Dimensional
Solidification and Bulging of Continuous Casting Slabs**

:

2001 2

**A Study of a Numerical Analysis on
Three-Dimensional Solidification and Bulging of
Continuous Casting Slabs**

Young-Dae Kim

**Department of Mechanical Engineering
Graduate School
Korea Maritime University**

Abstract

In the continuous casting process, the internal cracks should be prevented to achieve the improvement of productivity by high speed casting. The internal cracks can occur when tensile strains at the solidification front exceed a certain threshold level. The bulging of the strand is presumed to play a major role in occurrence of tensile strains that cause internal cracks. In particular, when the casting speed is high, strains caused by the bulging become large because of the decrease of the solidified shell thickness and the increase of the surface temperature of the strand.

In this paper, solidification analysis of strand-casting under air-mist spray condition, which uses air-mist mixture, is carried out by the two-dimensional finite difference method. In the solidification analysis, the boundary conditions of width face of slab are defined by considering

zones directly cooled by sprays and indirectly by rolls and radiation, and the boundary conditions of narrow face of slab are only defined by considering zones by radiation. In order to deal with complicated deformation of the slab, the three-dimensional elastic-plastic and creep models are used for analyzing bulging in the strand casting. The bulging deflections and strains are obtained by using the well-known finite element code ANSYS and are compared with those from the experiments under the same condition. For efficient bulging analysis, the output data of the finite difference method are automatically transformed to input data for ANSYS. The effects of important parameters in casting process of the slabs, such as casting speed, roll pitch and slab shape, are analyzed by implementation of the presented method.

When comparing with different casting speeds, the bulging strain obtained in the high speed casting appears to be larger than that at the low speed casting. Also, creep has great influence on the casting directional strain, which increases up to three times of the resulted value by the elasto-plastic model. Therefore, the effect of creep cannot be neglected in the computation of the bulging. When the ratio of width to thickness is smaller than 3.0, the values of casting directional strain and bulging deflection drastically decrease with decreasing of the slab width.

It is shown that the secondary cooling condition, roll pitch of the continuous caster and slab width are important process parameters to restrain the bulging and prevent the crack in high speed casting.

C	:	$[J/kg \cdot K]$
C_{eq}	:	$[J/kg \cdot K]$
L	:	$[J/kg]$
f_s	:	
α	:	$[m^2/s]$
\overline{T}_l	:	$[K]$
\overline{T}_s	:	$[K]$
\overline{T}_a	:	$[K]$
$\overline{T}_x, \overline{T}_y$:	$(\quad) [K]$
\overline{T}_o	:	$[K]$
t	:	$[s]$
ρ	:	$[kg/m^3]$
T	:	
h	:	$[W/m^2 \cdot K]$
\overline{T}_s	:	$[K]$
x, y	:	$[m]$
x_0, y_0	:	$[m]$
ε	:	(emissivity)
σ	:	Stefan-Boltzmann $(= 1.356 \times 10^{-12} [W/m^2 \cdot K^4])$
τ	:	

Abstract	i
.....	iii
List of Tables	vi
List of Figures	vii
1	1
1.1	1
1.2	2
1.3	4
2	7
2.1	8
2.2	9
2.3	10
2.4	12
2.5	15
2.5.1 1 ()	15
2.5.2 2	15
2.5.3	16
2.5.4	17
2.6	18
2.6.1	18
2.6.2	19

3	27
3.1	27
3.2	28
3.2.1	29
3.2.2	29
3.2.3	31
3.3	33
3.3.1	33
3.3.2	33
3.3.3	34
3.3.4	34
4	45
4.1	45
4.2	45
4.2.1	45
4.2.2	46
5	47
 	53

List of Tables

- Table. 1 The numerical data used for calculating the solidification of slab
- Table. 2 Chemical composition and thermophysical properties of casting steel
- Table. 3 Water flow rate for two cooling conditions
- Table. 4 Material properties at high temperature

List of Figures

- Fig. 1 A typical continuous caster
- Fig. 2 Lower right-hand quadrant of cross section of bar
- Fig. 3 Classification of secondary cooling zones
- Fig. 4 Temperature distribution of width face of slab
- Fig. 5 Temperature distribution of corner of slab
- Fig. 6 Temperature distribution of narrow face of slab
- Fig. 7 Variations of the y-directional solidified shell thickness with different casting speeds
- Fig. 8 Variations of the x-directional solidified shell thickness with different casting speeds
- Fig. 9 Temperature of solidified shell(casting speed=1.4m/min)
- Fig. 10 Temperature of solidified shell(casting Speed=2.0m/min)
- Fig. 11 Temperature distribution of width face of slab
- Fig. 12 Temperature distribution of corner of slab
- Fig. 13 Temperature distribution of narrow face of slab
- Fig. 14 Variations of the y-directional solidified shell thickness with different slab width length
- Fig. 15 Variations of the x-directional solidified shell thickness with different slab width length
- Fig. 16 Three-dimensional model in bulging analysis
- Fig. 17 Finite element mesh for bulging analysis
- Fig. 18 Uniaxial behavior for bilinear isotropic hardening and σ_k determination

- Fig. 19 Comparison of the measured bulging deflection with three analytical predictions [casting speed = 0.85m/min, shell thickness = 79 mm, slab width > 1300mm, roll pitch = 860mm]
- Fig. 20 Comparison between measured and calculated maximum bulging of roll pitch [casting speed=1.79m/min, slab width=1240mm, slab thickness=270mm]
- Fig. 21 Bulging deflection at distance from meniscus
- Fig. 22 Bulging strain at distance from meniscus
- Fig. 23 Effect of creep on bulging strains
- Fig. 24 Bulging deflection of slabs in the straightener roll zone with elasto-plasticity and creep
- Fig. 25 Bulging deflection of slabs in the straightener roll zone with different casting speeds
- Fig. 26 Strains of casting direction on the solidification front in the straightener roll zone
- Fig. 27 Variation of y-directional strain on solidification front at center of narrow face
- Fig. 28 Bulging deflection of slabs in the straightener roll zone with different width length [casting speed=1.4m/min, roll pitch=340mm]
- Fig. 29 Strains of slabs in the straightener roll zone with different width [casting speed=1.4m/min, roll pitch=340mm]
- Fig. 30 Schematic drawing of strand cast section showing different types of cracks
- Fig. 31 Width directional bulging strain (ϵ_x) distribution in the bender roll zone from meniscus
- Fig. 32 Thickness directional bulging strain (ϵ_y) distribution in the bender roll

zone from meniscus

Fig. 33 Casting-directional bulging strain(ε_z) distribution at in the bender roll

zone from meniscus

Fig. 34 Width directional bulging strain(ε_x) distribution in the straightener roll

zone from meniscus

Fig. 35 Thickness directional bulging strain(ε_y) distribution in the straightener roll

zone from meniscus

Fig. 36 Casting-directional bulging strain(ε_z) distribution in the straightener roll

zone from meniscus

1

1.1

. 19 Bessemer
(ingot)
1970

가
가
가
Fig. 1
, (ladle)
(strand)
가 (tundish)가
,
(bending) (straightening)
2
, 1
2 (strand)

가 (, ,
, ,) (heat size)

. HDR(hot direct rolling)

, .
, , .

가 .

.
.

. ,
가, 가 가 .

3 .

1.2

1950

가 .

. ,

(heat transfer coefficient)

[1-3],

가 가 [4].

1 [5-7].

2

가

傳野重行 [8]

2

가

Miyazawa [9]

(bending theory)

가

가

. Uehara [10]

(billet)

가

3

3

가

[12][13]. Grill [11]

가 1320

0.2% 0.3%

가

1.3

2 가

3

3

[10], 3

(creep)

2

3

(elasto-plastic)

(creep)

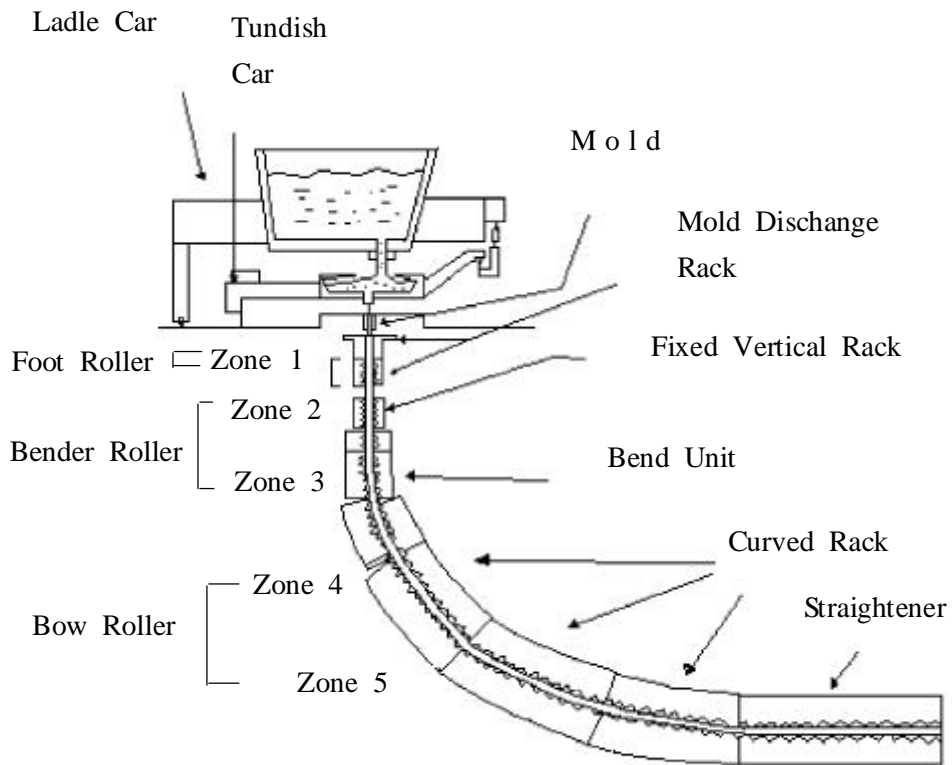


Fig. 1 A typical continuous caster

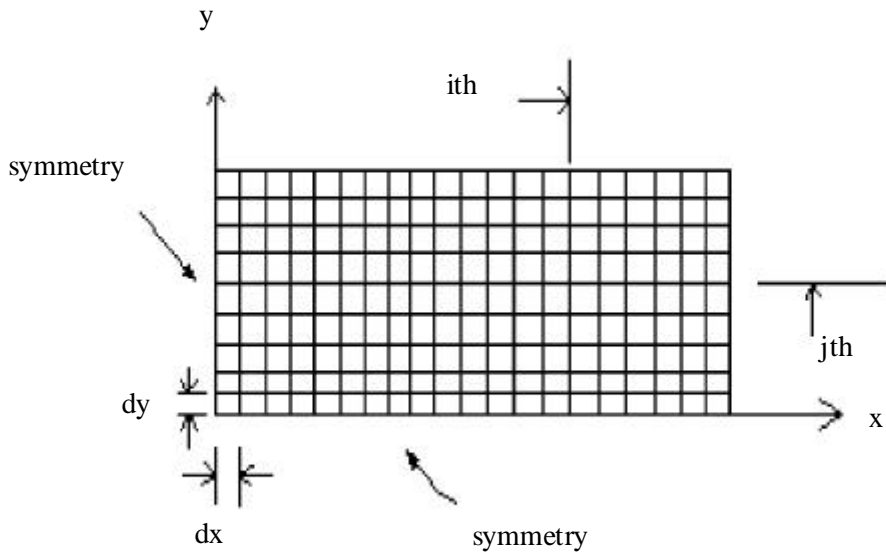


Fig. 2 Lower right-hand quadrant of cross section of bar

2

2

Table 1

Table 1 The numerical data used for calculating the solidification of slab

Parameters	Values	Units
Half slab thickness	125	mm
Slab width	1650, 250	mm
Mold length from meniscus	800	mm
Casting speed	1.4, 2.0	m/min
Roll temperature	100	
Heat transfer coefficient In roll contact	2500	W/m ² K
Emissivity of slab surface	0.9	
Cooling water temperature	30	
Initial temperature of casting material	1520.9	
Specific cooling water	0.45, 0.73	l/kg

2.1

- (1) 가 . 가 가 가 [14].
- (2) . . [15], 가 [16] 가 .
- (3) .

(4)

(enthalpy method) 가 (equivalent specific heat method)

가 30 가
[4][18]. 가

$$C_{eq} = C - L \frac{f_s}{t} = C + \frac{L}{T_1 - T_s} \quad (2.1)$$

2.2

(explicit) (implicit) (explicit)
($t + \Delta t$) , (preceding
time) t

가 Δt
 Δt

(implicit)

2.3

2

$$k \left(\frac{\partial^2 \bar{T}}{\partial x^2} + \frac{\partial^2 \bar{T}}{\partial y^2} \right) = \rho C \frac{\partial \bar{T}}{\partial t} \quad (2.2)$$

$$X = \frac{x}{x_0}, \quad Y = \frac{y}{y_0}, \quad T = \frac{\bar{T}_s - \bar{T}_a}{\bar{T}_0 - \bar{T}_r}, \quad \tau_x = \frac{\alpha(\bar{T}_x)t}{x_0^2}, \quad \tau_y = \frac{\alpha(\bar{T}_y)t}{y_0^2}$$

$$\frac{\partial^2 T}{\partial X^2} + \frac{\partial^2 T}{\partial Y^2} = \frac{\partial T}{\partial \tau} \quad (2.3)$$

Fig. 2

1/4 . , $\alpha (= k/\rho C)$, k , ρ
 , C , t , x_0, y_0
 , T_x, T_y (=) , T_0 .

, (p) (p+1)

가 . 2

i iteration

$$\frac{T_{i-1,j}^{p+1} - 2T_{i,j}^{p+1} + T_{i+1,j}^{p+1}}{(\Delta X)^2} + \frac{T_{i,j-1}^p - 2T_{i,j}^p + T_{i,j+1}^p}{(\Delta Y)^2} = \frac{T_{i,j}^{p+1} - T_{i,j}^p}{\left(\frac{\Delta \tau_x}{2}\right)} \quad (2.4)$$

$$- \lambda_1 T_{i-1,j}^{p+1} + (2\lambda_1 + 1)T_{i,j}^{p+1} - \lambda_1 T_{i+1,j}^{p+1} = \lambda_2 T_{i,j-1}^p + (1 - 2\lambda_2)T_{i,j}^p + \lambda_2 T_{i,j+1}^p$$

j iteration

$$\frac{T_{i-1,j}^p - 2T_{i,j}^p + T_{i+1,j}^p}{(\Delta X)^2} + \frac{T_{i,j-1}^{p+1} - 2T_{i,j}^{p+1} + T_{i,j+1}^{p+1}}{(\Delta Y)^2} = \frac{T_{i,j}^{p+1} - T_{i,j}^p}{\left(\frac{\Delta \tau_y}{2}\right)} \quad (2.5)$$

$$- \lambda_2 T_{i,j-1}^{p+1} + (2\lambda_2 + 1)T_{i,j}^{p+1} - \lambda_2 T_{i,j+1}^{p+1} = \lambda_1 T_{i-1,j}^p + (1 - 2\lambda_1)T_{i,j}^p + \lambda_1 T_{i+1,j}^p$$

$$\lambda_1 = \frac{\Delta \tau_x}{2(\Delta X)^2}, \quad \lambda_2 = \frac{\Delta \tau_y}{2(\Delta Y)^2}$$

.

x

$$\tau_x = 0 \quad T = T(x) \quad (2.6)$$

y

$$\tau_y = 0 \quad T = T(y) \quad (2.7)$$

x

$$1) X = 0 (x = 0), \quad \frac{T}{X} = 0 \left(\frac{T}{x} = 0 \right) \quad (2.8)$$

$$2) X = 1 (x = x_0), \quad \frac{T}{X} = - \frac{h x_0}{k} \frac{\overline{T_s} - \overline{T_a}}{\overline{T_0} - \overline{T_x}} \quad (2.9)$$

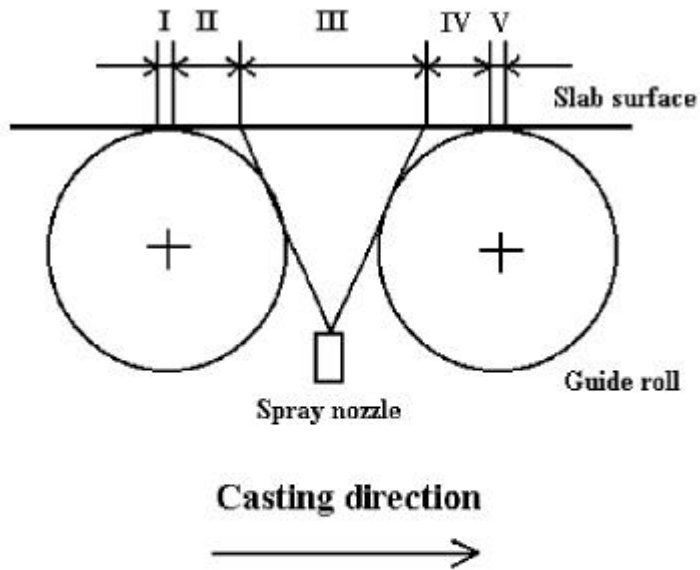
y

Table 2 Chemical composition and thermophysical properties of casting steel

Chemical composition	0.08% C, 0.25% Si, 1.55% Mn, 0.0% P, 0.0% S							
Liquid temperature	$T_L = 1536 - \{ 78 (\% C) + 7.6 (\% Si) + 4.9 (\% Mn) + 34.4 (\% P) + 38 (\% S) + 4.7 (\% Cu) + 3.1 (\% Ni) + 1.3 (\% Cr) + 3.6 (\% Al) \} = 1520.3$							
Solid temperature	$T_S = 1536 - \{ 415.5 (\% C) + 12.3 (\% Si) + 6.8 (\% Mn) + 124.5 (\% P) + 183.9 (\% S) + 4.3 (\% Ni) + 1.4 (\% Cr) + 4.1 (\% Al) \} = 1489.1$							
Density	7800 kg/cm ³							
Heat capacity	Temperature []	800	1200	1489.0	1489.1	1520.3	1520.4	1600
	kJ/kg ·	0.96	0.66	0.66	6.46	6.46	0.66	0.66
Thermal conductivity	Temperature []	800	1200	1489.1	1520.3	1600		
	W/m ·	28	30	30	30	30		

Table 3 Water flow rate for normal cooling conditions [l/min]

Cooling condition \ Zone	Zone 1	Zone 2	Zone 3	Zone 4	Zone 5
	Normal	450	320	292	458



I, V : Contact with roll

II, IV : Radiation

III : Spray cooling

Fig. 3 Classification of secondary cooling zones

2.5

2.5.1 1 ()

가

(meniscus)

Alvarez[1]

$$h_m(t) = ae^{-t} + be^{-t/n} + c \quad [\text{kcal/m}^2 \cdot \text{hr} \cdot] \quad (2.12)$$

$$, \quad t = \frac{z}{v}, \quad z, \quad v, \quad a =$$

$$0.07128, \quad b = 2.328, \quad c = 0.698, \quad n = 9.5$$

2.5.2 2

2

가 (guider roller)

(air-mist spray)

가

Fig. 3

가

[7].

2

(air-mist Spray)

10 μ m

가 . ,

,

2

가

가

가

Fand[19]가

$$h_{air} = 10^{1.48} \cdot \overline{T}_s^{-0.1358} \cdot \dot{W}^{0.6293} \cdot V_a^{0.2734} \quad [\text{kcal/m}^2 \cdot \text{hr} \cdot \text{]} \quad (2.13)$$

\overline{T}_s []

, \dot{W} [1/m² · min]

, V_a [m/sec]

가

2.5.3

(spray)

$$-k \frac{d\overline{T}}{dx} = \epsilon \sigma (\overline{T}_s^4 - \overline{T}_a^4) \quad (2.14)$$

$$-k \frac{d\bar{T}}{dx} = h_{rad} (\bar{T}_s - \bar{T}_a) \quad (2.15)$$

$$h_{rad} = \epsilon \sigma (\bar{T}_s^3 + \bar{T}_s^2 \bar{T}_a + \bar{T}_s \bar{T}_a^2 + \bar{T}_a^3) \quad (2.16)$$

2.5.4

2500W/m²K , 100 가
5mm
[20].

2.6

2.6.1

1650mm 가 240mm 1.4m/min,
2.0m/min . Fig. 4

, 가 가 가 2

가 . 2 가

, ,

, 15m

가 . Fig. 5

가 가 가 ,

가 . Fig. 6

, -

가 . Fig. 7 Fig. 8

. 1.4m/min 39.1m

, 2.0m/min

가 . Fig. 9 Fig. 10

가 .

2.6.2

1650mm 250mm 1.4m/min
가 , . Fig. 11

가 , ,
. Fig. 12

Fig. 13

가 . Fig. 14 Fig. 15

. 250mm 26m
가 1650mm 13m

가 .

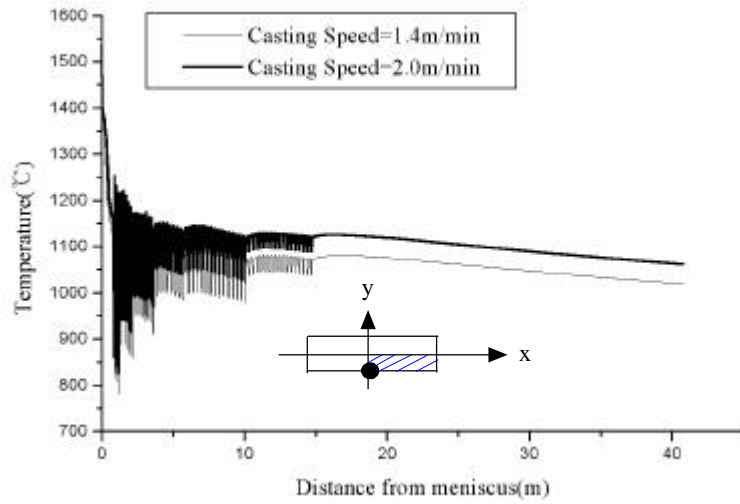


Fig. 4 Temperature distribution of width face of slab

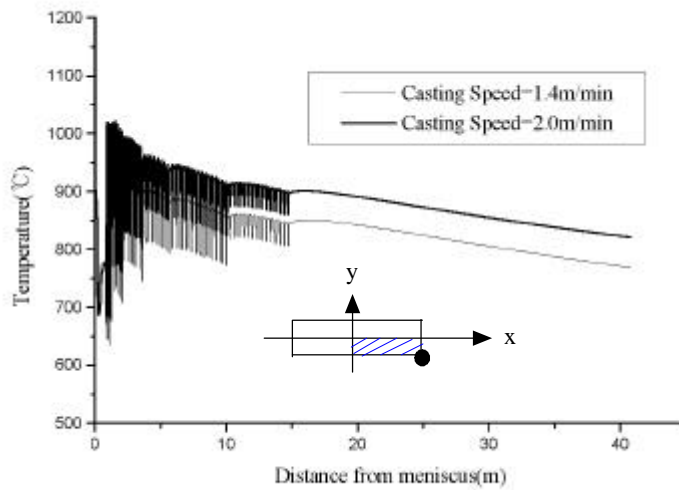


Fig. 5 Temperature distribution of corner of slab

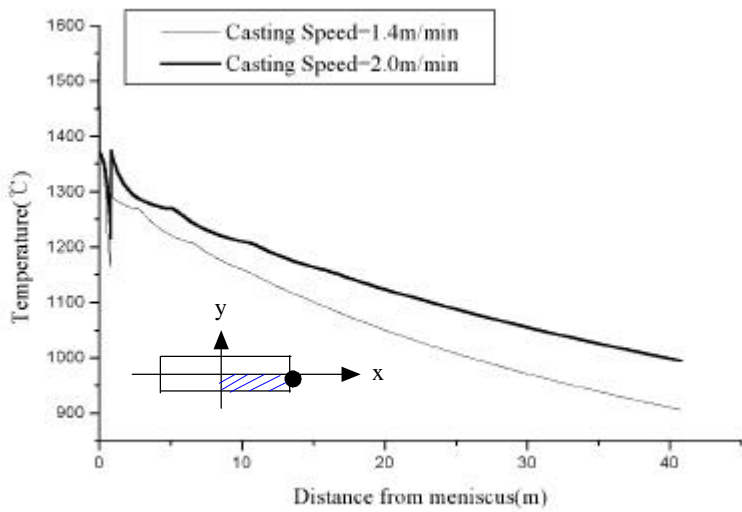


Fig. 6 Temperature distribution of narrow face of slab

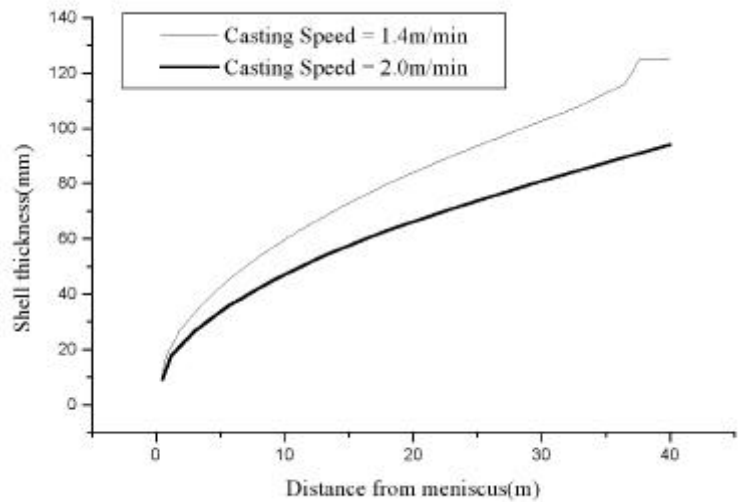


Fig. 7 Variations of the y-directional solidified shell thickness with different casting speeds

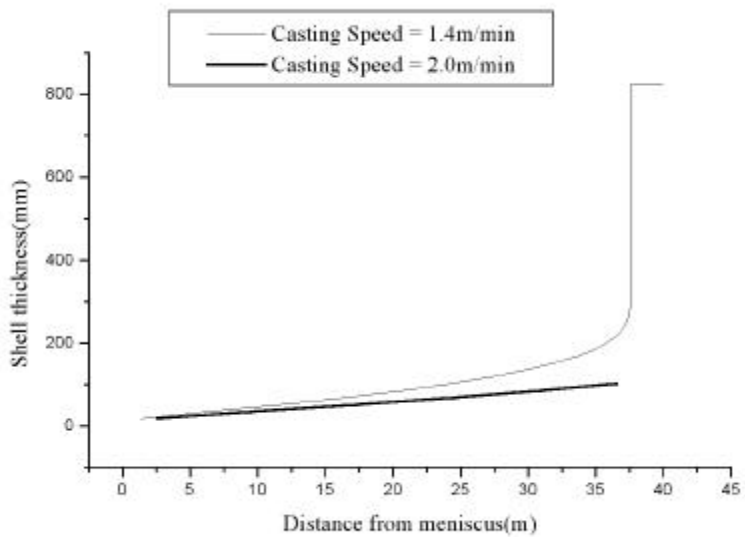


Fig. 8 Variations of the x-directional solidified shell thickness with different casting speeds

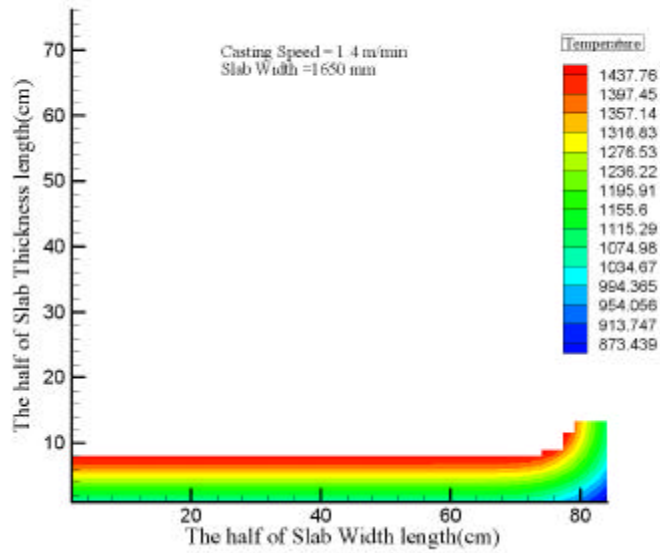


Fig. 9 Temperature of solidified shell(casting speed=1.4m/min)

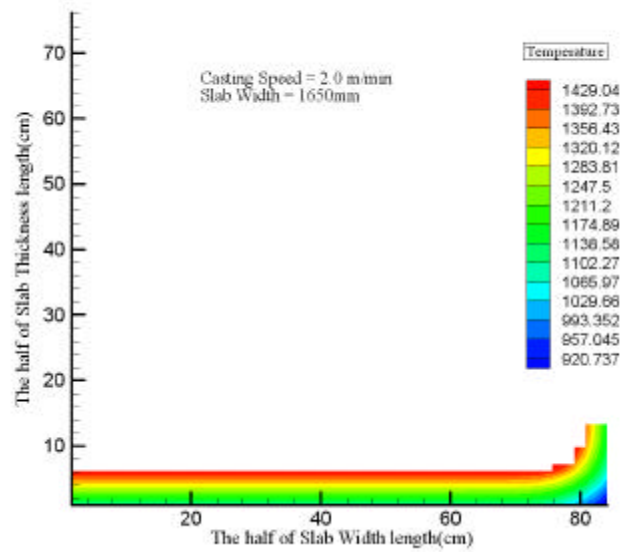


Fig. 10 Temperature of Solidified Shell(casting Speed=2.0m/min)

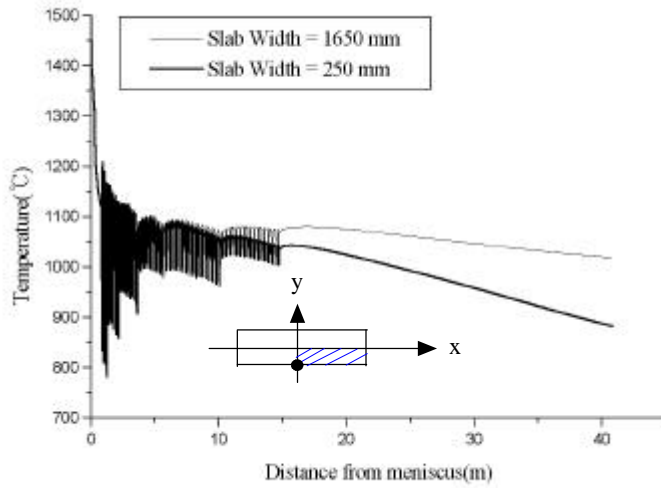


Fig. 11 Temperature distribution of width face of slab

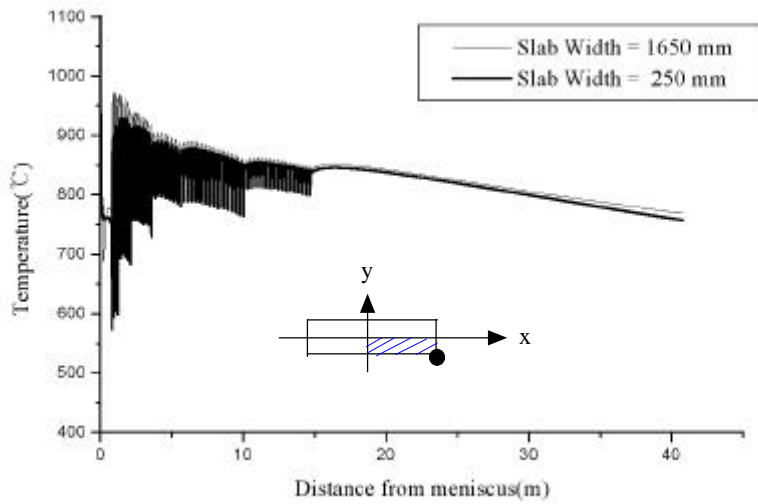


Fig. 12 Temperature distribution of corner of slab

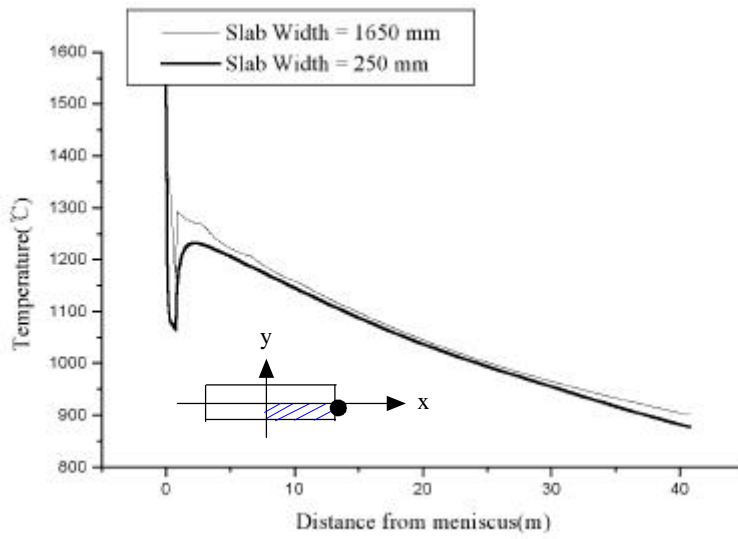


Fig. 13 Temperature distribution of narrow face of slab

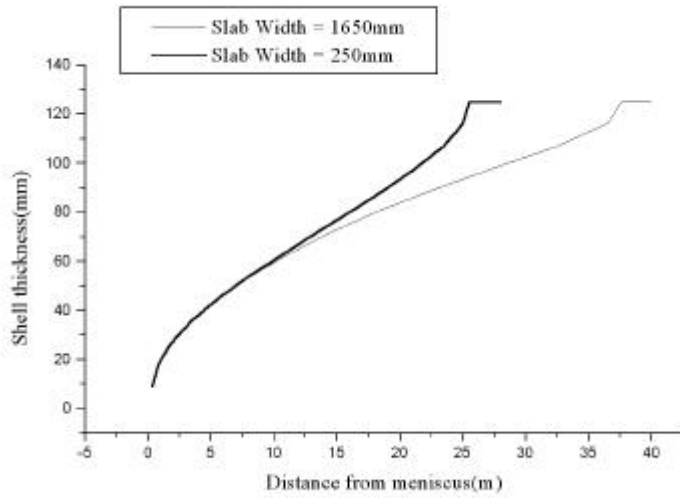


Fig. 14 Variations of the y-directional solidified shell thickness with different slab width length

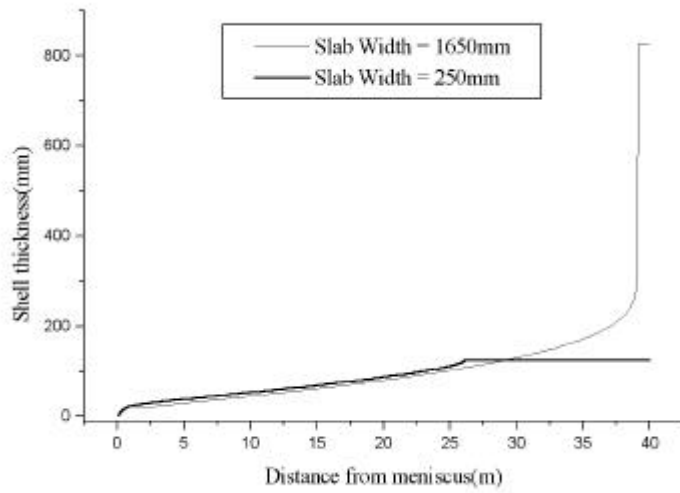


Fig. 15 Variations of the x-directional solidified shell thickness with different slab width length

3

ANSYS [21]

3

3.1

가

가

Fig. 20

Wümenberg

, Fig. 16

1/8

180 340mm ,

Fig. 17 8

ANSYS Solid45

[7].

Table 4

[22][23].

Table 4 Material properties at high temperature

Young's Modulus [MPa]	$E = 1.96 \times 10^4 - 18.375 (T - 1000)$ for $1000^\circ\text{C} < T < 1400^\circ\text{C}$ $E = 1.225 \times 10^4 (1475 - T) / 75$ for $1400^\circ\text{C} < T < 1475^\circ\text{C}$ $E = 0$ for $T > 1475^\circ\text{C}$ in $1 \times 10^{-4} \leq \dot{\epsilon} \leq 3 \times 10^{-1}$
Yield Stress [MPa]	$\sigma_y = 66.15 - 4.655 \times 10^{-2} T$ for $1000^\circ\text{C} < T < 1200^\circ\text{C}$ $\sigma_y = 54.39 - 3.675 \times 10^{-2} T$ for $1200^\circ\text{C} < T < 1480^\circ\text{C}$ $\sigma_y = 0$ for $T > 1480^\circ\text{C}$
Poisson's Ratio	0.33

3.2

3.2.1

2

$$[K^{(e)}] \{u^{(e)}\} = [f^{(e)}] \quad (3.1)$$

$$(3.1) \quad [K^{(e)}] \quad , \quad [f^{(e)}]$$

$$[K^{(e)}] = \int_v [B]^T [D] [B] dV \quad (3.2)$$

$[B]$

$$\{\epsilon\} = [B] \{u\} \quad (3.3)$$

3.2.2

(bilinear isotropic hardening) von Mises

가 (σ_e) (σ_k) ,

$$F = \left[\frac{3}{2} \{s\}^T [M] \{s\} \right]^{\frac{1}{2}} - \sigma_k = 0, \quad F = \sigma_e - \sigma_k = 0 \quad (3.4)$$

σ_k (W_p) .

$$\sigma_k = F(W_p) \quad (3.5)$$

(yield surface)

가 $\hat{\epsilon}^{p1}$ Fig. 18

$$\hat{\epsilon}_n^{p1} = \hat{\epsilon}_{n-1}^{p1} + \Delta \hat{\epsilon}^{p1} \quad (3.6)$$

$\hat{\epsilon}_n^{p1}$ 가 , $\hat{\epsilon}_{n-1}^{p1}$

가 가 .

$$d\{\sigma\} = [D^{ep}] d\{\epsilon^{el} + \epsilon^{p1}\} \quad (3.7)$$

$[D^{ep}]$ (instantaneous) -

$$[D^{ep}] = [D^e] - \frac{[D^e]\{s\} ([D^e]\{s\})^T}{(H\{\sigma\})^T \{s\} + \{s\}^T [D^e]\{s\}} \quad (3.8)$$

H .

$$H = \frac{2}{3} \left(\frac{E E_T}{E - E_T} \right) \quad (3.9)$$

E_T Fig. 18 (strain-hardening modulus)

$$E_T = 0.1E$$

3.2.3

가 (creep strain rate) $\dot{\epsilon}_{cr}$, ANSYS 가 [21]

$$\Delta\epsilon^{cr} = \dot{\epsilon} \Delta t \tag{3.10}$$

$$\dot{\epsilon} = C_1 \sigma^{C_2} t^{C_3} \exp(-C_4/T) ; C_6 = 1 \tag{3.11a}$$

$$\dot{\epsilon} = C_1 \sigma^{C_2} \epsilon^{C_3} \exp(-C_4/T) ; C_6 = 0 \tag{3.11b}$$

$\Delta\epsilon^{cr}$: (creep strain increment)

$\dot{\epsilon}$: (average strain rate)

Δt : (time increment)

C_1 C_4 : (constant values from the creep test)

Fig. 19

Wünnenberg [24]

. Fig. 19

Matsumiya [26] (3.12) 가

Matsumiya 가 10

$$\dot{\epsilon} [1/s] = 0.0806 \exp \{ - 28392 / (T + 273) \} \cdot \{ \sigma [kg / cm^2] \}^{3.15} \quad (3.12)$$

Fig. 20

Wünnenberg [24]

가 .

, (3.12) C₁ C₄ ANSYS .

$$C_1 = 0.0806, C_2 = 3.15, C_3 = 0, C_4 = 28392$$

$$t_{cr} = \frac{1}{2} \cdot \frac{L}{V} [22][27] \quad (3.13)$$

t_{cr}, L, V , , .

3.3

1650mm 가 250mm
250mm
. 40m
가 가
Fig. 21 Fig. 22
15.82m y ϵ_z 가 15.48m

3.3.1

Fig. 20
900mm 가 가 가
가 .

3.3.2

Fig. 23
(zero) ,

, 가 ϵ_z 가
 ϵ_x, ϵ_y . Fig. 24

, 0.12mm ,
 0.35mm 가 가 .
 가 가

3.3.3

Fig. 25

가 가 . Fig. 26
 15.48m 가

가 ,

가 .

3.3.4

Fig. 27 y

ϵ_y 가

가 .

가

가

. Fig. 28 2 3

770mm

2

3

가

가

가 250mm

3

ϵ_y 2 가 가 . Fig. 29 ϵ_x ,
 ϵ_z
 , ϵ_z 가
 ϵ_x , ϵ_y 가 가 .

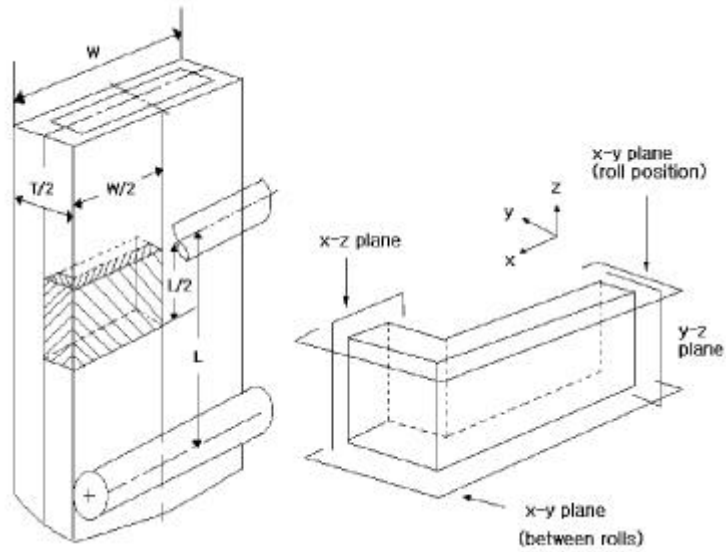


Fig. 16 Three-dimensional model in bulging analysis.

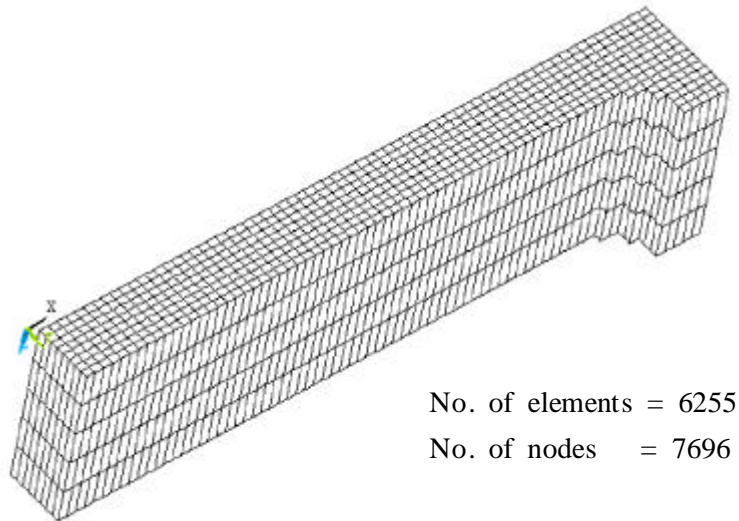


Fig. 17 Finite element mesh for bulging analysis

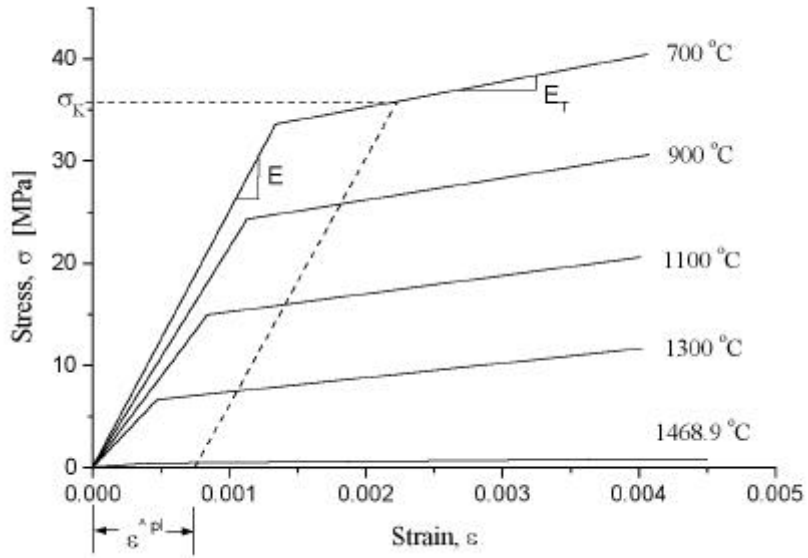


Fig. 18 Uniaxial behavior for bilinear isotropic hardening and σ_k determination

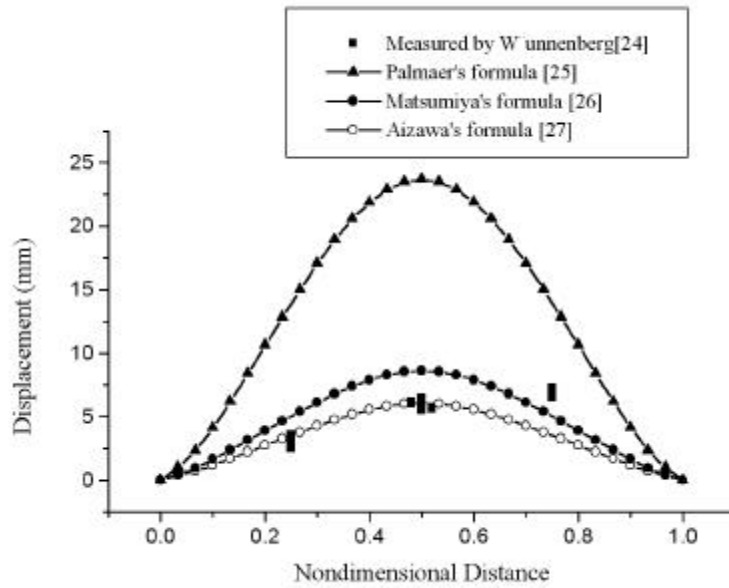


Fig. 19 Comparison of the measured bulging deflection with three analytical predictions [casting speed = 0.85m/min, shell thickness = 79mm, slab width > 1300mm, roll pitch = 60mm]

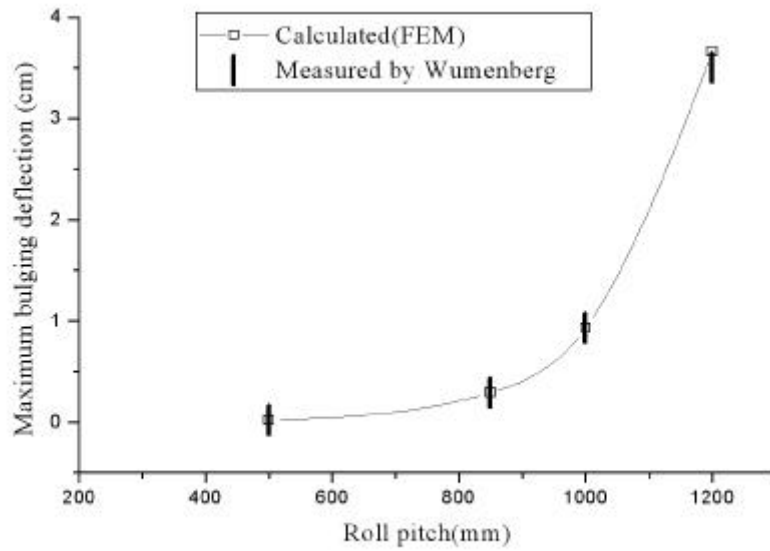


Fig. 20 Comparison between measured and calculated maximum bulging with roll pitch [casting speed = 1.79m/min, slab width=1240mm, slab thickness = 270mm]

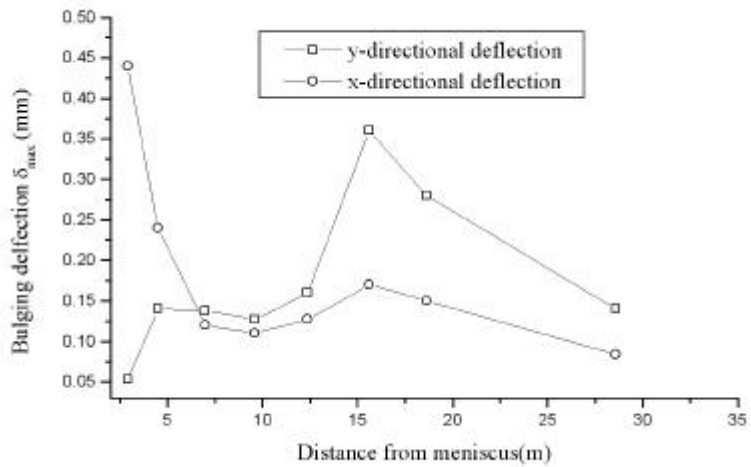


Fig. 21 Bulging deflection at distance from meniscus [casting speed = 1.4m/min, slab width=1650mm, slab thickness = 250mm]

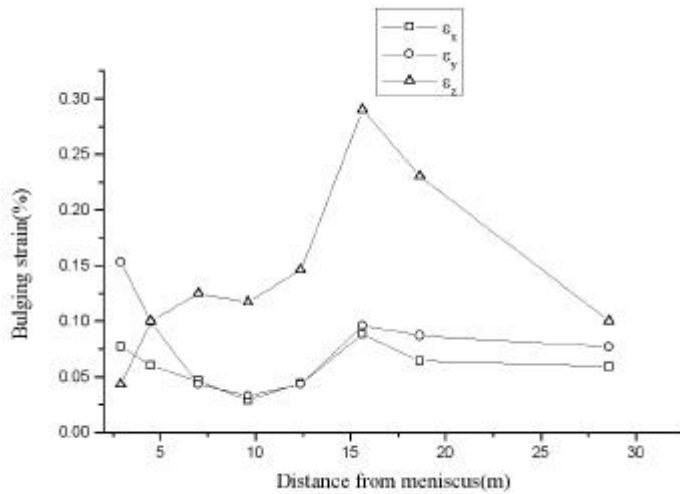


Fig. 22 Bulging strain at distance from meniscus [casting speed = 1.4m/min, slab width=1650mm, slab thickness = 250mm]

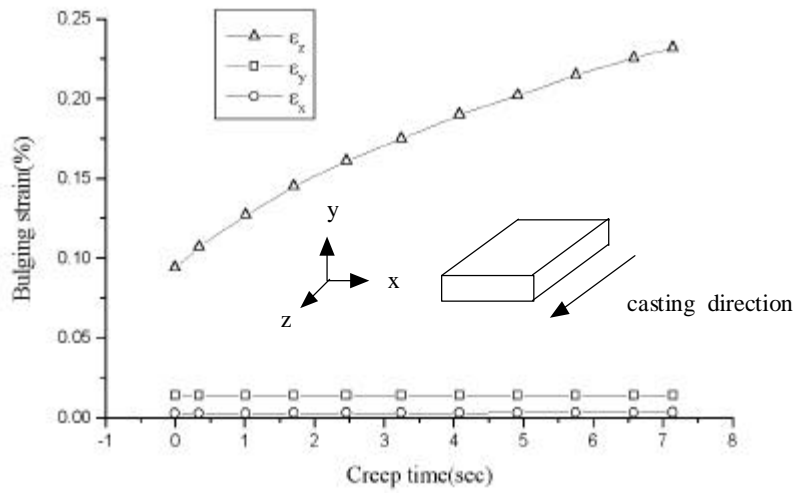


Fig. 23 Effect of creep on bulging strains [casting speed = 1.4m/min, slab width=1650mm, slab thickness = 250mm]

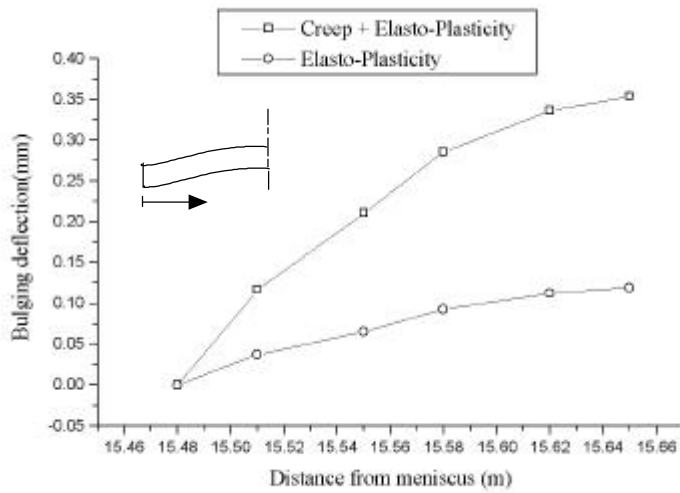


Fig. 24 Bulging deflection of slabs in the straightener roll zone with elasto-plasticity and creep [casting speed = 1.4m/min, slab width=1650mm, slab thickness = 250mm]

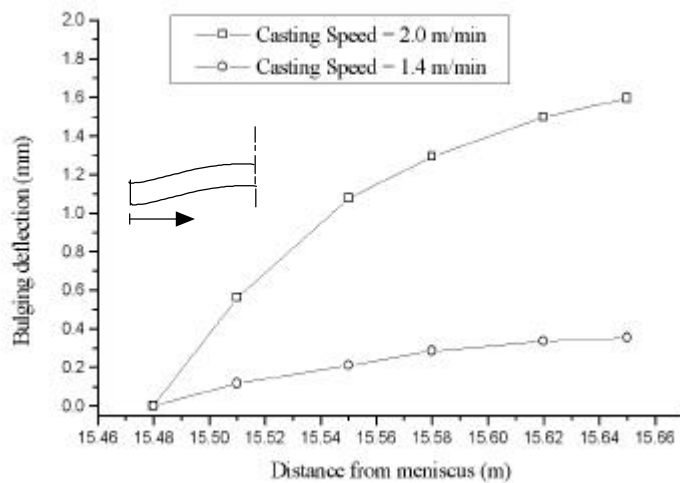


Fig. 25 Bulging deflection of slabs in the straightener roll zone with different casting speeds [slab width=1650mm, slab thickness = 250mm]

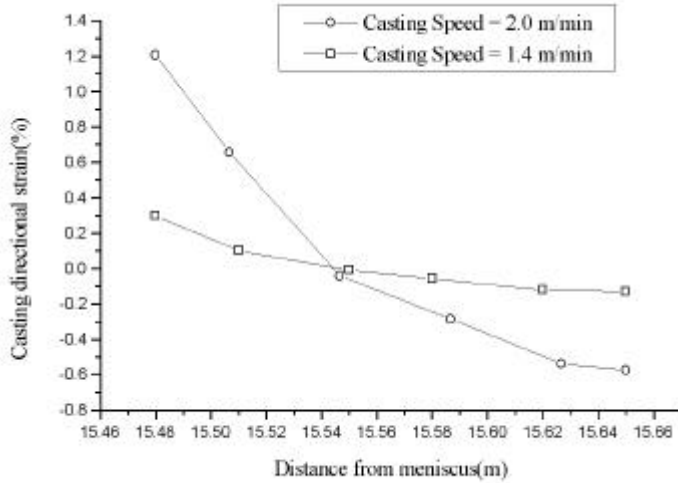


Fig. 26 Strains of casting direction on the solidification front in the straightener roll zone [slab width=1650mm, slab thickness = 250mm]

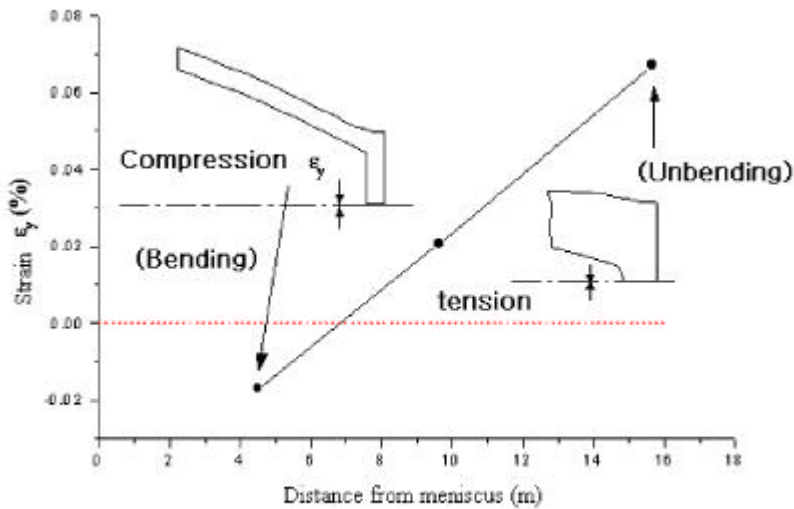


Fig. 27 Variation of y-directional strain on solidification front at center of narrow face [casting speed = 1.4m/min, slab width=1650mm, slab thickness = 250mm]

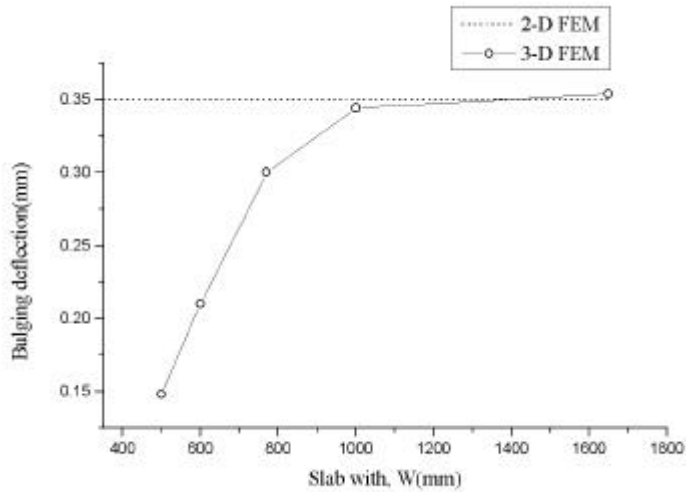


Fig. 28 Bulging deflection of slabs in the straightener roll zone with different width length [casting speed = 1.4m/min, roll pitch=340mm]

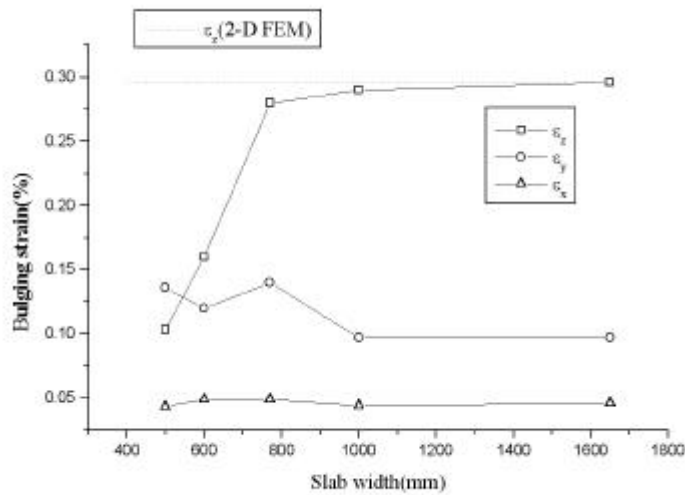


Fig. 29 Strains of slabs in the straightener roll zone with different width [casting speed=1.4m/min, roll pitch = 340mm]

4

4.1

Fig. 30

[28]

Fig. 30

(pinch roll)

1340

가

2 3

5

6

가

4.2

4.2.1

Fig. 31

Fig. 33

3m

$\epsilon_x, \epsilon_y,$

ϵ_z

x

가

y

x ϵ_x y ϵ_y z ϵ_z

0.15% Grill [11]

4.2.2

Fig. 34 Fig. 36 15m

$\epsilon_x, \epsilon_y, \epsilon_z$. Fig. 34 x

ϵ_x 가 가 , Fig. 35 y

ϵ_y 가 가

. Fig. 36 ϵ_z 가

가 .

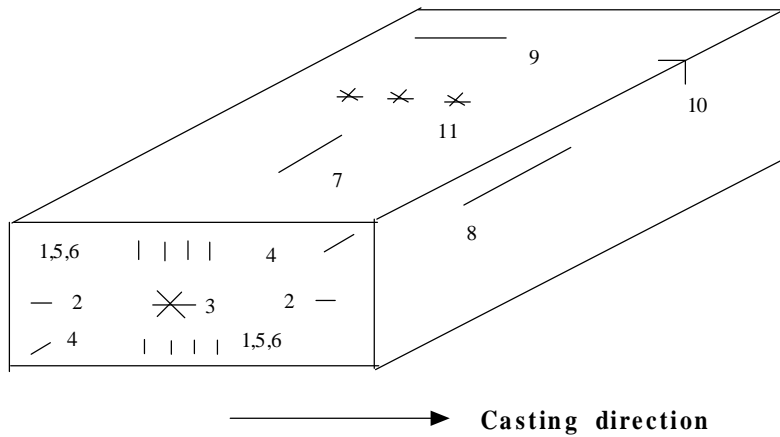
Fig. 30

1,5,6 2 .

0.29%

. Grill [11]

가 가 .



Cracks in continuously cast steel

Internal cracks

1. Midway
2. Triple-point
3. Centreline
4. Diagonal
5. Straightening / bending
6. Pinch roll

Surface cracks

7. Longitudinal, mid-face
8. Longitudinal, corner
9. Transverse, mid-face
10. Transverse, corner
11. Star

Fig. 30 Schematic drawing of strand cast section showing different types of cracks

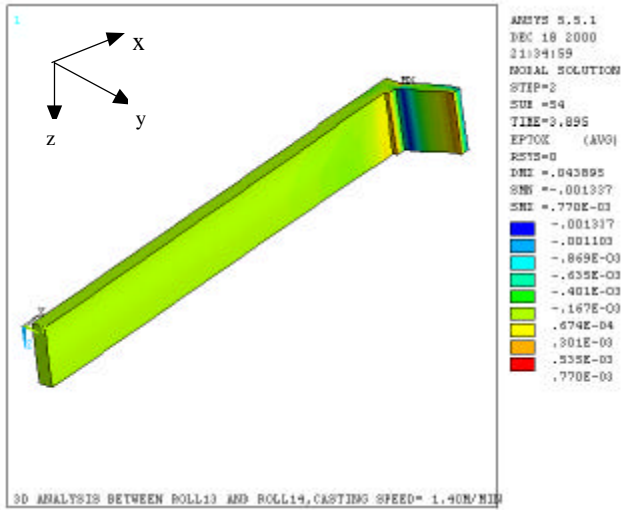


Fig. 31 Width directional bulging strain(ϵ_x) distribution in the bender roll zone from meniscus

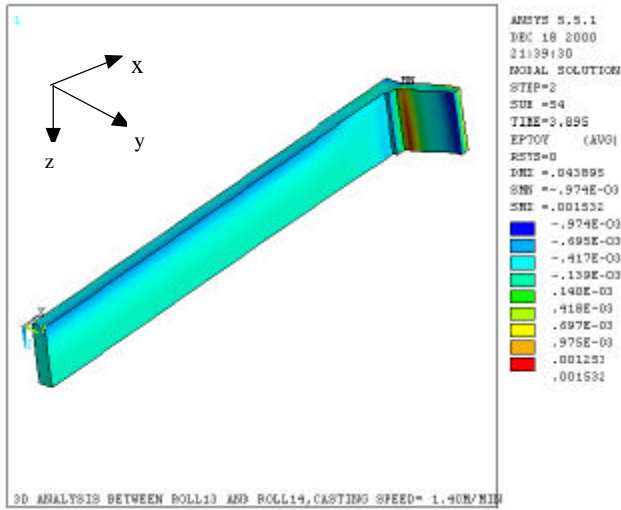


Fig. 32 Thickness directional bulging strain(ϵ_y) distribution in the bender roll zone from meniscus

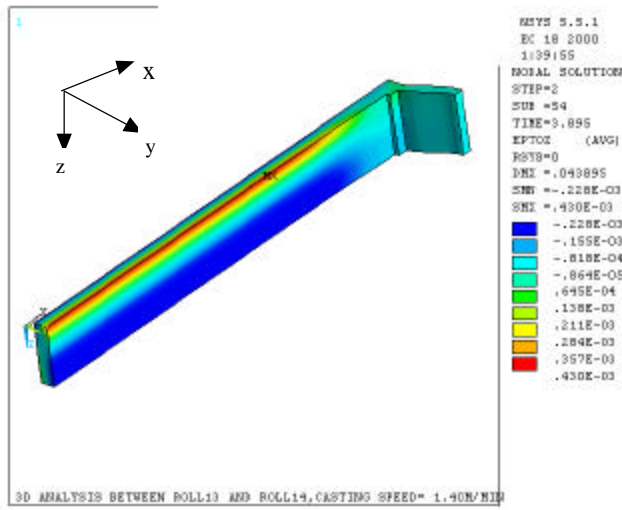


Fig. 33 Casting-directional bulging strain(ϵ_z) distribution at in the bender roll zone from meniscus

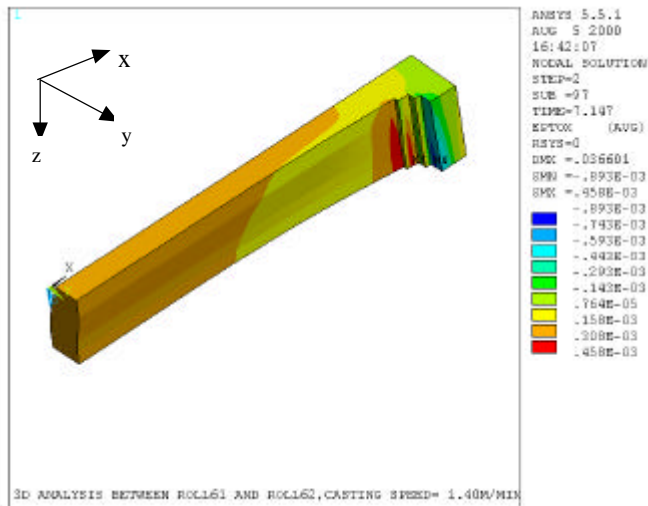


Fig. 34 Width directional bulging strain(ϵ_x) distribution in the straightener roll zone from meniscus

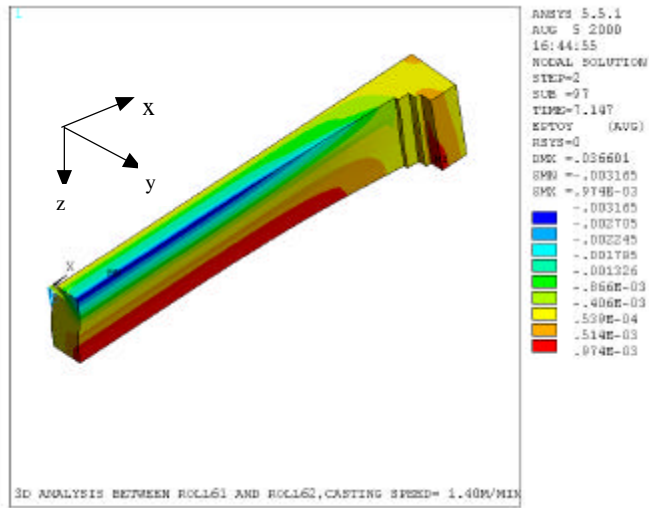


Fig. 35 Thickness directional bulging strain(ϵ_y) distribution in the straightener roll zone from meniscus

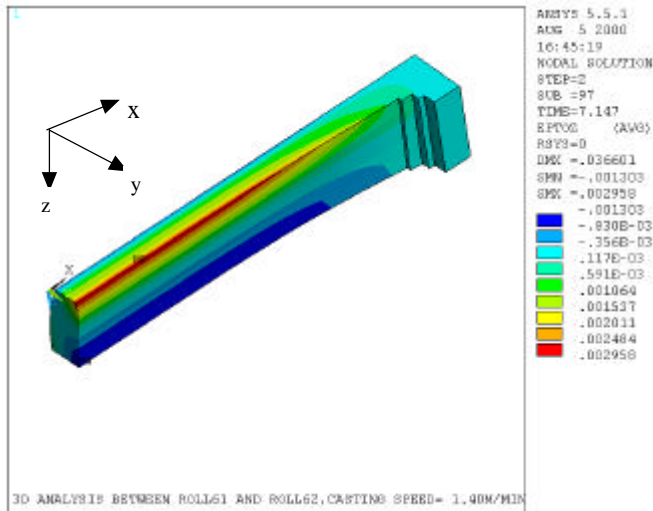


Fig. 36 Casting-directional bulging strain(ϵ_z) distribution in the straightener roll zone from meniscus

- [1] G. Alvarez de Toledo, J. Lainez and J. C. Cirion, 1993, Model optimization of continuous casting steel secondary cooling, Elsevier Sequoia, pp.287-291.
- [2] , , , , , , 1991, , , Vol. 29, No. 12, pp.1197-1205 .
- [3] N.M. Vanaparthi and M.N. Srinivasan, 1994, "Simulation of Solidification in Continuous Cast Steel Using Finite Element Method," ASME, HTD-Vol. 289, pp.131-138.
- [4] M. El-Bealy, N. Leskinen and H. Fredriksson, 1995, Simulation of cooling conditions in secondary cooling zones in continuous casting process, Ironmaking and Steelmaking, Vol. 22, No. 3, pp.246-255 .
- [5] J. Matsuno, H. Nakano, H.Ooi, "An Analysis of Solidification Rate and Surface Temperature of Continuous Casting Slabs", Journal of The Iron and Steel Institute of Japan, Vol. 60, No. 7, pp.285-294, 1974
- [6] K. Miyazawa, I. Muchi, "Theoretical Analysis on the Solidification Profiles of Slab in Circular-arc Type Continuous Casting Machine, Journal of The Iron and Steel Institute of Japan, Vol. 62, No. 2, pp.269-274, 1976
- [7] , , 2000, , , 17 11 , pp. 122-128.
- [8] 前野重行, 和田 要, 1985, 連鑄鑄片バルジングの測定と考察, 連鑄鑄造における力學的舉動 鐵鋼基礎共同研究會 連鑄鑄造に おける力學的舉動部會, pp.124-127.
- [9] K. Miyazawa and K. Schwerdtfeger, 1979, Computation of bulging of continuously cast slabs with simple bending theory, Ironmaking and

- Steelmaking, No. 2, pp.68-74
- [10] M. Uehara, I. V. Samarasekera and J. K. Brimacombe, 1986, Mathematical modeling of unbending of continuously cast steel slabs, Ironmaking and Steelmaking, Vol. 13, No. 3, pp.138-153.
- [11] A. Grill, J. K. Brimacombe and F. Weinberg, 1976, Mathematical analysis of stresses in continuous casting of steel, Ironmaking and Steelmaking, No. 1, pp.38-47.
- [12] K. Okamura and H. Kawashima, 1989, Three-dimensional Elasto-Plastic and Creep Analysis of Bulging in Continuously Cast Slabs, ISIJ International, Vol. 29, No. 8, pp.666-672.
- [13] A. Grill and K. Schwerdtfeger, 1979, Finite-element analysis of bulging produced by creep in continuously cast steel slabs, Ironmaking and Steelmaking, No. 3, pp.131-135.
- [14] A.W.D. Hills: J. Iron Steel Inst., 203 (1965) 18
- [15] J.E. Lait, J.K. Brimacombe and F. Weinberg: Ironmaking Steelmaking, I (1974) 90
- [16] K. Cliff and R.J. Dain: J. Iron Steel Inst., 205 (1967) 1186
- [17] E. A. Mizikar, 1974, Mathematical Heat Transfer Model for Solidification Profiles of Slab in Circular-arc Type Continuous Casting Machine, 鐵と鋼, Vol. 60, pp.1007-1012.
- [18] M. SALCUDEAN, Z. ABDULLAH, 1988, On The Numerical modelling of Heat Transfer During Solidification Processes, INTERNATIONAL JOURNAL FOR NUMERICAL METHODS IN ENGINEERING, Vol. 25, pp 445-473
- [19] R .M. Fand, 1965, Int, J. Heat Mass Transfer, Vol. 8, pp.995.
- [20] B. Barber, B. A. Lewis and B. M. Leckenby, 1985, Finite-element analysis of strand deformation and strain distribution in solidifying shell during

- continuous slab casting, Ironmaking and Steelmaking, Vol. 12, No. 4, pp.171-175.
- [21] ANSYS User's Manual Theory Part
- [22] K. Miyazawa and K. Schwerdtfeger, 1972, Computation of bulging of continuously with simple bending theory, Ironmaking and Steelmaking, No. 2, pp.68-74 .
- [23] K. Fukawa, H. Matsumoto and K. Nakajima, 1982, Rheological Analysis of Bulging of Continuously Cast Slabs with Elementary Bending Theory, 鐵と鋼, Vol. 68, No. 7, pp.86-90.
- [24] K. Wünnenberg and Duisburg - Huckingen, 1978, Strand bulging between supporting rollers during continuous slab casting, Stahl u. Eisen, Vol. 98, No. 6, pp.254-259 .
- [25] A.Palmaers, 1979, CRM, No. 53, pp.23.
- [26] 松宮徹, 梶岡傳幸, 中村泰, 1982, 連続鑄片バルジングの數學的解析, 製鉄研究, No. 310, pp.14951-14957.
- [27] T. Aizawa, G. Yakawa and I. Ohnaka, 1985, Metallurgy and Mechanics of Continuous Casting, Joint Soc. on Iron and Steel Basic Research of ISIJ, ISIJ, Tokyo, pp.145.
- [28] J. K. BRIMACOMBE AND K. SORIMACHI Crack Formation in the Continuous Casting of Steel, METALLURGICAL TRANSACTIONS, Vol. 8B, September 1977